Evidence for a chemical-thermal structure at base of mantle from sharp lateral P-wave variations beneath Central America

Xinlei Sun*, Xiaodong Song*†‡, Sihua Zheng†, and Don V. Helmberger‡§

*Department of Geology, University of Illinois at Urbana–Champaign, Urbana, IL 61801; †Institute of Earthquake Science, China Earthquake Administration, Beijing 100036, China; and §Seismological Laboratory, California Institute of Technology, Pasadena, CA 91125

Contributed by Don V. Helmberger, October 23, 2006 (sent for review May 18, 2006)

Compressional waves that sample the lowermost mantle west of Central America show a rapid change in travel times of up to 4 s over a sampling distance of 300 km and a change in waveforms. The differential travel times of the PKP waves (which traverse Earth's core) correlate remarkably well with predictions for S-wave tomography. Our modeling suggests a sharp transition in the lowermost mantle from a broad slow region to a broad fast region with a narrow zone of slowest anomaly next to the boundary beneath the Cocos Plate and the Caribbean Plate. The structure may be the result of ponding of ancient subducted Farallon slabs situated near the edge of a thermal and chemical upwelling.

core–mantle boundary | slab

Global seismic tomography has produced consistent images of very large-scaled seismic structure of Earth's mantle over the last decade. However, details of smaller-scaled structure, such as slabs and plumes, differ. Resolution of these small-scaled structures are important in understanding the material circulation and the thermal and chemical structure of the mantle. In particular, these differences make it difficult to address unambiguously the issue of whether the subducted slabs penetrate to the lower mantle, the mid-mantle, or the lowermost mantle (1–6), or the issue of whether plumes rise up from the lowermost mantle to the surface (7–9).

One of the most consistent features in global tomography is slab-like high-velocity anomalies in both P and S waves to the depth of at least 1,200 km underneath the Americas (2, 3, 10–13). As early as 1974, Jordan and Lynn (14) had identified anomalously high P and S velocities in the lower mantle beneath the Caribbean. Although P tomographic studies have poorest resolution on the lowermost mantle because of limited sampling, S-wave studies clearly show fast broad anomalies in the lowermost 500 km of the mantle beneath Central America (e.g., ref. 3). Extensive high-resolution studies of the deepest mantle in this area have been conducted over the years (15–27). The data are S waveforms from earthquakes in South America recorded in North America stations, providing a dense sampling of a narrow corridor of the lowermost mantle beneath the Caribbean and the Cocos Plate. The region was found to have complex structures with a S velocity discontinuity, broad fast anomalies, anisotropy, and a possible ultra-low velocity zone at the base of the mantle. Detailed studies of P-wave structure of this region have been limited (18, 19, 27). Here we show rapid variation of P-wave velocity in the lowermost mantle from a broad fast anomaly underneath the Caribbean and much of the Cocos Plate to a broad slow anomaly to the southwest. The P anomalies correlate well with S velocity anomalies.

Data

Our data set contains high-quality broadband digital seismograms of compressional waves that traverse Earth's core, known as PKP waves (Fig. 1). Precise relative times were measured manually by using waveform correlation between PKP(DF) (traversing the inner core) and PKP(AB) (turning in mid-outer core), after correcting for Hilbert transform in the AB phase. The data come from earthquakes in South America recorded at the China Seismograph Network (CSN) (a national backbone network of broadband stations installed in recent years) and from earthquakes in Western Pacific recorded at a few stations in South America (Fig. 2) at distances of ≈149° to 177°. The PKP data set used here has several advantages. (*i*) Our data provide a dense coverage over a large area in the lowermost mantle beneath the Caribbean as well as the adjacent regions. The coverage also provides a rare case for part of our study area in which dense samplings of both P and S waves are available. (*ii*) Because the AB path is similar to the DF path in the upper mantle but is much more grazing in the lowermost mantle (Fig. 1), differential AB-DF times are not sensitive to upper mantle heterogeneity or errors in source location but are very sensitive to the lowermost mantle heterogeneity (30, 31). The level of heterogeneity in the D″ region (about the bottom 250 km of the mantle) is known to increase near the core–mantle boundary, boosting the sensitivity to lowermost mantle structure [supporting information (SI) Fig. 5]. (*iii*) The influence of inner core anisotropy on the DF travel times is small for these equatorial paths (29).

PKP Travel-Time Anomalies and Correlation with S Model

Our basic observation is that differential AB-DF travel times change rapidly along ray paths sampling beneath Central America (Figs. 1 and 2, and SI Fig. 6). The largest variation is between the AB paths that cross a boundary near the southwestern edge of the Cocos Plate (hereafter referred to as the "Cocos Boundary") (Fig. 2*A*). The Cocos Boundary corresponds to the azimuths of about −45° to about −30° from South American earthquakes recorded at the CSN. The AB-DF residuals decrease by 2–4 s over this narrow azimuthal range (Fig. 2*B*). The rapid change can be seen directly in individual recordings at the CSN (Fig. 1*B*, and SI Fig. 6). When aligned on the DF phase, the AB phase appears clearly faster at the azimuths greater than −30° than those at azimuths less than that. In addition, its waveform appears more variable and often more complex as the AB speeds up.

The changes in travel times and waveforms are observed from both shallow and deep events (SI Fig. 6), suggesting that upper mantle slabs are unlikely to be the cause (30). To understand the

Author contributions: X. Song and D.V.H. designed research; X. Sun and X. Song performed research; X. Sun and S.Z. analyzed data; and X. Sun, X. Song, and D.V.H. wrote the paper.

The authors declare no conflict of interest.

Abbreviations: CC, cross-correlation coefficient; CSN, China Seismograph Network.

‡To whom correspondence may be addressed. E-mail: xsong@uiuc.edu or helm@gps.caltech.edu.

This article contains supporting information online at www.pnas.org/content/full/0609143103/DC1.

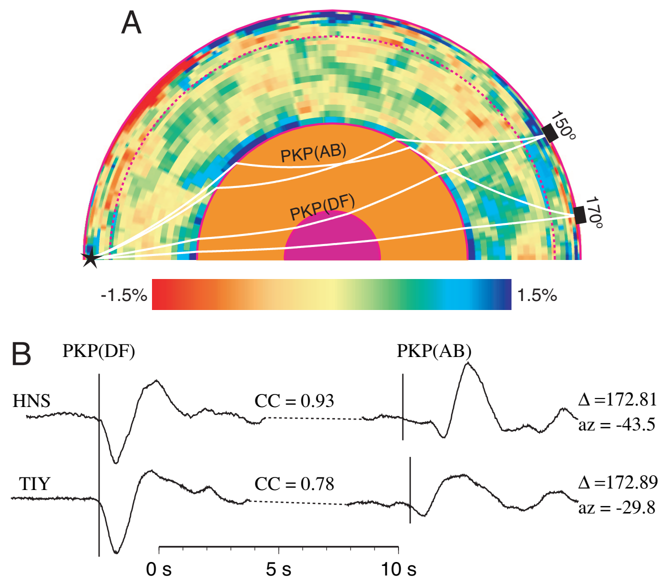

Fig. 1. Display of ray paths for PKP branches DF and AB along with examples of observed waveforms. (*A*) The ray paths are from a shallow earthquake (star) to two stations (squares) at distances of 150° and 170°. The background is Grand's S tomographic model along the azimuth of about −25° from South America to China. The half circles are the surface, 660 discontinuity, core–mantle boundary, and inner-core boundary. (*B*) The data are vertical components of ground velocity from the same earthquake in South America (March 15, 2001; lat 32.32°S, long 71.49°W; 37 km, body-wave magnitude of 5.6) recorded at two stations (HNS and TIY) of the CSN at about the same distance but slightly different azimuths. The traces are aligned with the DF arrivals, and the amplitudes are normalized relative to the DF phase. A segment of the same length (indicated by the dotted line) is removed from both traces for better visualization of the DF and AB arrivals. (The differential AB-DF time is ≈87 s at this distance.) The time marks before the DF and AB arrivals show the relative arrival times for the PREM model (28). The example also provides a good demonstration of the key observations of this study. When aligned with the DF, the AB arrival of TIY is clearly faster than that of HNS (by ≈1.1 s). The AB waveform of TIY is also anomalously broader than that of HNS, reducing the CC of DF and AB (Hilbert) from 0.93 at HNS to 0.78 at TIY.

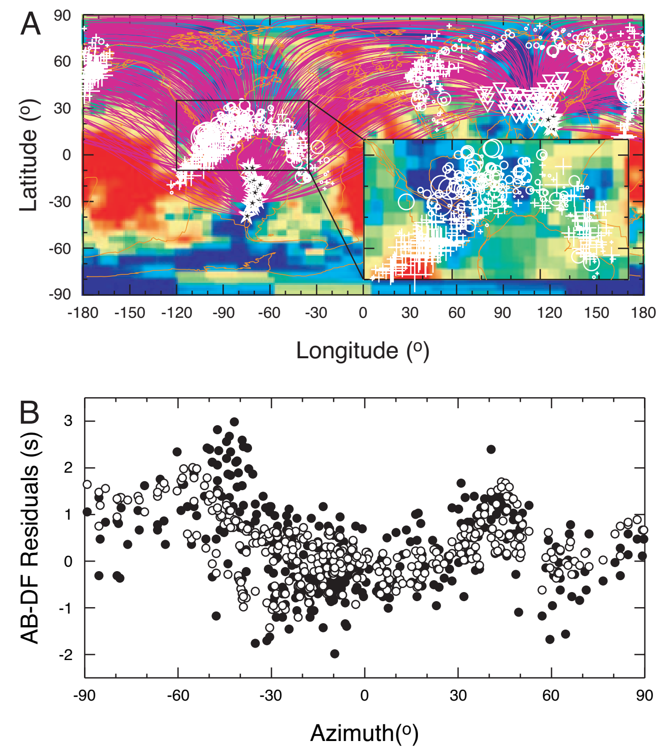

Fig. 2. PKP data used in this study. Our data consist of 435 AB-DF measurements from 45 events recorded at 65 permanent and portable stations. Most of the data (90%) are from earthquakes in South America (total 28) recorded at 47 stations of the CSN. Additional data are from earthquakes in the Western Pacific recorded at portable stations and a few permanent stations in South America that were used previously (29). (*A*) Surface projection of ray paths. Earthquakes and stations are stars and inverted triangles, respectively. Residuals of differential AB-DF travel times with respect to PREM are plotted at the crossing points of the PKP(AB) rays at the core–mantle boundary. Positive and negative residuals are indicated by the crosses and circles, respectively, and the symbol size is proportional to the size of the residual. (The largest symbols correspond to approximately +3 s and −2 s, respectively.) In the background is the latest tomographic image of S velocity perturbations from S. Grand (3). (*Inset*) Blow-up of the Central America region of particular interest in this study. (*B*) Observed (filled circles) and predicted (open circles) differential AB-DF residuals as a function of azimuth for earthquakes in South America recorded at the CSN. The predictions, based on Grand's model and scaled by a factor of 0.52, match the observations reasonably well, but the observed decrease around −45° to −30° is significantly sharper.

source of our anomalies, we compare the observed differential-time residuals with predictions for the S tomographic model by S. Grand (3) (his latest version) in Fig. 2*B* where the agreement is remarkable. A linear regression of our data with Grand's predictions yield a slope of 0.520 ± 0.025 (SI Fig. 7), which reduces the data variance by 52%. The cross-correlation coefficient (CC) of our data and Grand's predictions is 0.72. Because of the completely different types of data and ray paths, the high correlation is significant and allows us to use the scaled Grand model with a scaling factor of $\mathrm{dln}V_p/\mathrm{dln}V_s$ of 0.52 as a 3D reference model (hereafter referred to as the "reference 3D model") for modeling our PKP data (which sample mostly the lowermost mantle regions outside the "superplumes" beneath Africa and the Central Pacific). Comparing the predicted DF, AB, and AB-DF perturbations for source-side (beneath the Americas) and station-side (beneath Asia) of the mantle shows clearly that, although part of the observed anomalies such as the increased residuals at azimuths of 40° to 50° (Fig. 2*B*) comes from the Asian side of the mantle, most of the decrease in the AB-DF residuals from −90° to −40° azimuths to −30° to 0° azimuths comes from the lowermost mantle part of the AB paths at the American side (SI Fig. 8). For this azimuth range (−90° to 0°), the AB, DF, and AB-DF from the American side of the mantle reduce the variance of the predicted total AB-DF times by 72%, 2%, and 82%, respectively, and the CCs with the total AB-DF times are 0.85, 0.15, and 0.91, respectively. The observed azimuthal variation is the result of the sampling of the broad slow anomaly southwest of the Cocos Plate and the Caribbean fast anomaly at the base of the mantle (Fig. 2*A Inset*).

Modeling Results

The most significant discrepancy between our data and the 3D reference model is at azimuths of −50° to −30°, where the P-data indicate the largest contrast between the slow-fast velocities and a sharp transition in between. To model this structure, we correct the observed AB-DF residuals for the 3D reference model and use the corrected residuals to map velocity perturbations uniformly along the AB paths in the lowermost part of the American side of the mantle. The velocity perturbations for all of the rays are then averaged by using the same parameterization as the reference 3D model (horizontal 2° × 2° grids and vertical layers), which are in turn added to the 3D reference model to make our final P model. Our data coverage does not allow us to constrain uniquely the depth distribution of the corrected residuals. However, sensitivity tests on the Grand model suggest that our data are mostly sensitive to the bottom 500 km of the mantle (SI Fig. 5). We choose the bottom four

GEOPHYSICS

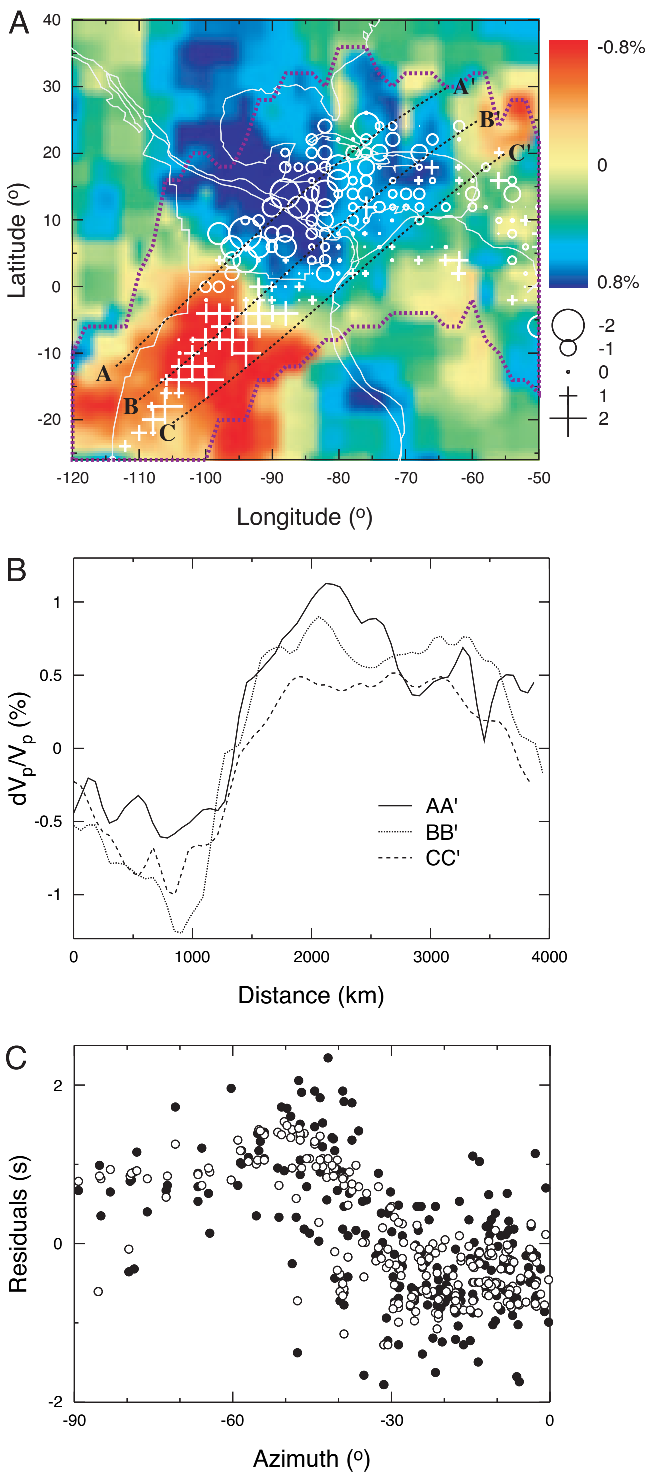

Fig. 3. Display of our P velocity model and its predictions. (*A*) P velocity for the D″ layer (depth 2,650–2,891 km). Only the region inside the dashed lines is constrained by our data; the area outside is the reference 3D model (Grand's model scaled by a factor of 0.52). Symbols are observed AB-DF residuals plotted at the middle of the ray segments in this layer. The residuals have been corrected for the 3D reference model at the Asian side of the ray path. The corrected residuals are then binned at 2° × 2°. (*B*) P velocity perturbations along the profiles AA′, BB′, and CC′ indicated in *A*. (*C*) Fit of predicted travel-time perturbations for our P model (open circles) to the observed AB-DF residuals (filled circles) as a function of azimuths from South America events to China. The data have been corrected for the Asian side of the mantle as in *A*, and the predictions include only the contributions from the American side of the mantle.

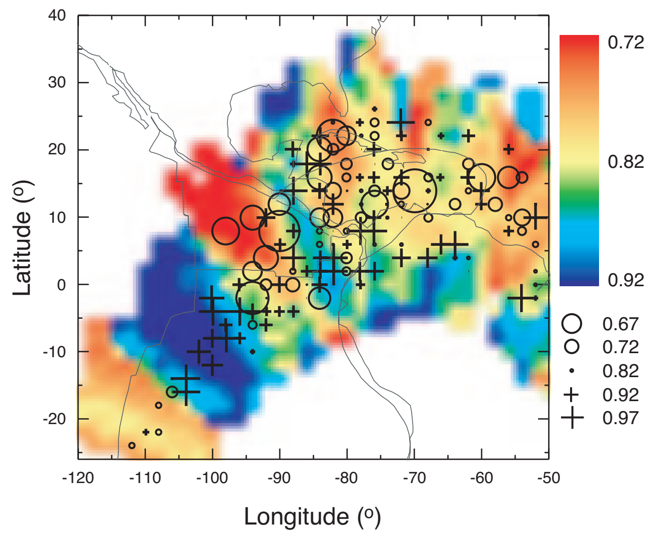

Fig. 4. Map of normalized CCs of observed DF and AB waveforms. The normalized CC values (relative to the highest CC value of each event) are mapped on to the D″ layer (lowermost 241 km) that are sampled by the AB rays under the Central America (color). The values averaged over 2° × 2° grids are plotted at the middle of the AB segment in the layer (symbols).

layers of Grand's model (or the lowermost 691 km of the mantle) for our mapping (Fig. 3 and SI Fig. 9).

We focus on the bottommost layer, the D″ layer, where the PKP(AB) path becomes the most grazing and our data are most sensitive to lateral variation at this depth. Our model for the D″ layer (Fig. 3*A*) is marked by the contrast of a very fast region underneath the Caribbean and much of the Cocos Plate and a very slow region to the southwest. The boundaries of fast region are well delineated in the west (at approximately lat 15°N, long 108°W to lat 4° S, long 88°W), in the south (at approximately lat 4°S, long 88°W to lat 17°N, long 62°W), and in the east (at approximately lat 17°N, long 62°W to lat 35°N, long 77°W). The northern boundary is further north of our sampling area and thus not constrained by our data. The fast region appears to be a continuous structure covering ≈2,000 km west to east and at least comparable length south to north with a total area of >4 million km^2. Thus, if the P and S anomalies are correlated as they appear to be at least in our study area, the two fast regions in the underlying Grand model (Fig. 2*A*) are in fact connected. Similarly, the slow region to the southwest is also a large structure as it appears in the original S model. The transition from slow to fast (the Cocos Boundary) is sharp over an ≈200- to 300-km sampling distance, which is easier to see along the marked three profiles (Fig. 3*B*). The velocity jump is ≈1.5–2.2%. The model fits the data reasonably well (Fig. 3*C*), improving the variance reduction to 67% over that of 41% from the reference 3D model. Near the Cocos Boundary, there is a narrow zone of particularly low velocity, as indicated in profiles AA′ and BB′ at the distance of ≈800–900 km. The observed large residuals at azimuths −50° to −40° indicate that this slow velocity zone may be sharper (narrower with even slower velocities) than what can be accommodated with our simple parameterization of relatively coarse grids and thick layers. Although less pronounced, the velocity increase from south to north is also clear. From profile CC′ to profile AA′, the velocity increases by ≈0.6% in the region just east of the Cocos Boundary (Fig. 3*C*). The observed residuals decrease by ≈1 s from ≈0° in the south to ≈20° in the north, and the model predictions fit the trend well (SI Fig. 10). Our velocity structure, which is controlled by the rapid variation in the data, is robust. The amplitude of our velocity jump (1.5–2.2%) across the Cocos Boundary, however, depends on our assumption of the depth distribution of the corrected differential-time residuals. If they are distributed over the bottom 1,400 km of the mantle, the jump changes very little (decrease by ≈0.2%); if they are distributed over the bottom 240 km of the mantle, the jump increases by ≈0.5%.

Changes in Waveforms

We also observe significant changes in the AB waveforms as they sample the fast region (Figs. 1 and 4, and SI Fig. 6). The AB waveforms are more complex and variable compared with those sampling the slow region to the southwest. We quantify this by mapping the CCs of DF and AB waveforms onto the D″ layer (Fig. 4). The mapping procedure is similar to that of mapping the velocity perturbations. To account for different source time histories, we selected 24 events in South America with relatively simple source time functions and recorded by many stations. The highest CC for each event is larger than ≈0.8. The CCs of all of the records of each event are then normalized by the highest value of that event. The average of the normalized CC is ≈0.82. We see a clear decrease of the CCs across the Cocos Boundary from the slow region to the fast region. The location of the boundary of the CC change matches remarkably well with that of the velocity change. The CCs also decrease noticeably from south to north as the AB rays sample the fast region under the Cocos Plate and the Caribbean. The CC inside the fast region is variable but generally about or lower than the average.

Discussion and Conclusion

The causes of large anomalies in the lowermost mantle are uncertain. They could be thermal, chemical, or phase change (32, 33). The relative behavior of P and S velocities in the mantle can be used to infer mantle properties (10) because of different sensitivities of bulk and shear moduli to temperature and chemical composition (34). Our P data correlate well with raw predictions for Grand's S tomographic model. If we use the original amplitudes of S-velocity perturbations in Grand's model, we estimate the ratio $R = \mathrm{dln}V_s/\mathrm{dln}V_p$ to be ≈1.9 (SI Fig. 7). This value is not anomalous, comparable with values for mid-mantle and significantly less than estimated global average of 2.5 or larger for the lowermost mantle (which probably indicates chemical heterogeneity) (10). The estimate, however, has considerable uncertainty, because the level of heterogeneity is strongly influenced by data sampling and smoothing and weighting in a tomographic inversion. On the other hand, the region is densely sampled by S waves in the lowermost mantle. Grand's model fits observed ScS and S differential travel times and waveforms sampling this region quite well (24, 25), suggesting that the level of heterogeneity of the model for the lowermost mantle is probably appropriate on average. Joint modeling of P and PKP data and S data sampling this region is required to constrain better the *R* value.

The bimodal structure that we found with broad fast and slow anomalies in both P and S velocities separated by a sharp boundary appears distinctly different from anomalies away from subduction zone, beneath the Africa and the Central Pacific. Sharp transitions in S velocity in the lowermost mantle are also found at the edges of the "African anomaly" (e.g., refs. 35 and 36) and at the southern border of the "Pacific superplume" (37). However, the P velocity anomaly is quite small compared with the large S velocity anomaly under Africa (38). The *R* value in the lowermost mantle beneath the Central Pacific region is identified to be particularly anomalous, and the bulk sound velocity is anticorrelated with S velocity. Global P tomographic models generally show fast anomalies in the D″ under the Central America [see the recent review by Romanowicz (39)]. However, some P models (40–42) also show that the high velocities extend west across the Pacific at mid-northern latitudes, which is not present in S models. These observations may suggest different natures and dynamical regimes between our structure and those under Africa and the Central Pacific. The narrow zone of particularly low velocities near the Cocos Boundary in our model may also suggest that the broad slow anomaly in the eastern Pacific that is connected to an even broader slow anomaly under Central Pacific in global tomographic models may be more closely associated with the fast anomaly underneath Central America than with the Central Pacific slow anomaly. Our results show clearly the existence of fast P-velocity anomalies in the lowermost mantle under the Caribbean and the Cocos Plate, in addition to fast S-velocity anomalies found previously. This large volume of fast P and S anomalies may represent a graveyard of the ancient subducted Farallon slab (e.g., refs. 20 and 24). Using deep earth migration techniques, Hutko *et al.* (26) discovered a sudden jump in D″ discontinuity across about the same location of our southern boundary and slow anomalies to the west, consistent with our velocity jump across the Cocos Boundary. Following the basic approach of Sidorin *et al.* (32) by imposing a phase change induced by temperature anomalies, Sun and Helmberger (25) found an enhanced phase boundary in the D″ from anomalously triplicated S waveforms at a locality slightly to the east. Both studies have suggested the presence of folded slabs in the lowermost mantle, which are consistent with the fastest velocities under the Cocos Plate and Central America in our model. The observed PKP(AB) waveform complication is also consistent with the presence of complex slab structure. Strong lateral velocity variations at the base of the mantle have been demonstrated to cause ray bifurcation with multipaths containing slow and fast contributions to PKP(AB) waveforms (43). However, chemical change seems required to explain the sharp Cocos Boundary. Dynamical simulations suggest that plumes preferentially develop at the edge of slabs (44) or that metastable superplumes with sharp edges develop in a thermochemical convection involving materials of higher density and bulk modulus than the ambient mantle (45). Thus, our velocity structure may be a combination of thermal, chemical, and phase change effects. One possibility is that our observed sharp boundary and the anomalously slow narrow region near the boundary may be the result of subducted Farallon slabs sweeping thermal chemical plumes onto the edge of the slabs. Alternatively, our broad slow region may be part of the Pacific superplume. The narrow zone of even slower anomalies near the Cocos Boundary may be the manifestation of the superplume at its edge.

This work benefited from constructive reviews by Vernon Cormier and Barbara Romanowicz and discussion with Mike Gurnis, Don Anderson, and Daoyuan Sun. We thank Alex Hutko and Thorne Lay for preprints. This work was supported by the National Science Foundation and the Natural Science Foundation of China. This is contribution no. 9164 of the Division of Geological and Planetary Sciences, California Institute of Technology.

1. Wysession ME (1996) *Nature* 382:244–248.
2. Karason H, van der Hilst RD (2001) *J Geophys Res* 106:6569–6587.
3. Grand SP (2002) *Philos Trans R Soc London A* 360:2475–2491.
4. Kellogg LH, Hager BH, van der Hilst RD (1999) *Science* 283:1181–1184.
5. Wen LX, Anderson DL (1998) *Earth Planet Sci Lett* 146:367–377.
6. Fukao Y, Widiyantoro S, Obayashi M (2001) *Rev Geophys* 39:291–323.
7. Anderson DL (2005) in *Plates, Plumes, and Paradigms*, eds Foulger GR, Natland JH, Presnall DC, Anderson DL (Geol Soc Am, Boulder, CO), Special Paper 388, pp 31–54.
8. van der Hilst RD, de Hoop MV (2005) *Geophys J Int* 163:956–961.
9. Montelli R, Nolet G, Dahlen FA (2006) *Geophys J Int* 167:1204.
10. Masters TG, Laske G, Bolton H, Dziewonski AM (2000) in *Earth's Deep Interior: Mineral Physics and Tomography from the Atomic to the Global Scale*, eds Karato S, Forte AM, Liebermann RC, Masters G, Stixrude L (Am Geophys Union, Washington, DC), AGU Geophys Monogr 117, pp 63–87.
11. Megnin C, Romanowicz B (2000) *Geophys J Int* 143:709–728.
12. Gu YJ, Dziewnski AM, Su WJ, Ekstrom G (2001) *J Geophys Res* 106:11169–11199.

GEOPHYSICS

13. Ritsema J (2005) in *Plates, Plumes, and Paradigms*, eds Foulger GR, Natland JH, Presnall DC, Anderson DL (Geol Soc Am, Boulder, CO), Special Paper 388, pp 11–18.
14. Jordan TH, Lynn WS (1974) *J Geophys Res* 79:2679–2685.
15. Lay T, Helmberger DV (1983) *Geophys J R Astron Soc* 75:799–838.
16. Kendall JM, Nangini C (1996) *Geophys Res Lett* 23:399.
17. Kendall JM, Silver PG (1996) *Nature* 381:409.
18. Ding XM, Helmberger DV (1997) *Phys Earth Planet Inter* 101:245–270.
19. Reasoner C, Revenaugh J (1999) *J Geophys Res* 104:955–961.
20. Garnero EJ, Lay T (2003) *Phys Earth Planet Inter* 140:219–242.
21. Fisher JL, Wysession ME, Fischer KM (2003) *Geophys Res Lett* 30, 10.1029/2002GL016179.
22. Lay T, Garnero EJ, Russell SA (2004) *Geophys Res Lett* 31, 10.1029/2004GL020300.
23. Thomas C, Garnero EJ, Lay T (2004) *J Geophys Res* 109, 10.1029/2004JB003013.
24. Hung SH, Garnero EJ, Chiao LY, Kuo BY, Lay T (2005) *J Geophys Res* 110, 10.1029/2004JB003373.
25. Sun DY, Song TR, Helmberger DV (2006) *Geophys Res Lett* 33, 10.1029/2005GL025384.
26. Hutko AR, Lay T, Garnero EJ, Revenaugh J (2006) *Nature* 441:333–336.
27. Ren Y, Stutzmann E, van der Hilst RD, Besse J (2006) *J Geophys Res*, in press.
28. Dziewonski AM, Anderson DL (1981) *Phys Earth Planet Inter* 25:297–356.
29. Sun XL, Song XD (2002) *Earth Planet Sci Lett* 199:429–445.
30. Song XD, Helmberger DV (1997) *Geophys Res Lett* 24:1863–1866.
31. Bréger L, Tkalcic H, Romanowicz B (2000) *Earth Planet Sci Lett* 175:133–143.
32. Sidorin I, Gurnis M, Helmberger DV (1999) *Science* 286:1326–1331.
33. Murakami M, Hirose K, Kawamura K, Sata N, Ohishi Y (2004) *Science* 304:855–858.
34. Karato S-I, Karki B (2001) *J Geophys Res* 106:21771–21783.
35. Masters G, Johnson S, Laske G, Bolton H (1996) *Philos Trans R Soc London A* 354:1385–1410.
36. Helmberger DV, Lay T, Ni SD, Gurnis M (2005) *Proc Natl Acad Sci USA* 102:17257–17263.
37. To A, Romanowicz B, Capdeville Y, Takeuchi N (2005) *Earth Planet Sci Lett* 233:137–153.
38. Wen LX, Silver P, James D, Kuehnel R (2001) *Earth Planet Sci Lett* 189:141–153.
39. Romanowicz B (2003) *Annu Rev Earth Planet Sci* 31:303–328.
40. Bijwaard H, Spakman W, Engdahl ER (1998) *J Geophys Res* 103:30055–30078.
41. Obayashi M, Fukao Y (1997) *J Geophys Res* 102:17825–17841.
42. Tkalcic H, Romanowicz B, Houy N (2002) *Geophys J Int* 149:599–616.
43. Luo SN, Ni SD, Helmberger DV (2001) *Earth Planet Sci Lett* 189:155–164.
44. Tan E, Gurnis M, Han LJ (2002) *Geochem Geophys Geosyst* 3, 10.1029/2001GC000238.
45. Tan E, Gurnis M (2005) *Geophys Res Lett* 32, 10.1029/2005GL024190.